Preprint Volume, Symposium on the 50th. Anniversary of Operational Numerical Weather Prediction, American Meteorological Society, University of Maryland, College Park, MD, 20pp, 14-17 June, 2004.

P2.9 THE NRL MOUNTAIN WAVE FORECAST MODEL (MWFM)

Stephen D. Eckermann
Middle Atmosphere Dynamics Section, Naval Research Laboratory, Washington, DC

Jun Ma, Dave Broutman
Computational Physics, Inc., Springfield VA

1. INTRODUCTION

The Department of Defense (DoD) has a large and increasing investment in high-altitude long-endurance (HALE) reconnaissance aircraft. First developed in the mid-late 1950's, the Air Force (AF) still makes extensive use of its U-2 spy planes. More recently, the Air Force and now the Navy are accumulating fleets of Global Hawk Unmanned Aerial Vehicles (UAVs). HALE aircraft such as these cruise at altitudes ~60,000-70,000 feet (FL600-700; heights z~20 km or atmospheric pressures p~50 hPa), roughly twice as high as commercial fleets. U-2 flights can last up to 6-8 hours, while Global Hawk can remain airborne for up to 42 hours which, given air speeds ~150-200 m s^{-1}, gives these airframes nearly global range.

HALE aircraft have lightweight broad-winged designs that both maximize lift and minimize extraneous weight, enabling them to reach stratospheric altitudes (Schawe et al. 2002). These properties make them both aerodynamically and structurally vulnerable to any severe turbulence they intercept at altitude. Since the stratosphere is very dry and thus has no *in situ* cloud-related sources of turbulence from severe weather, only clear-air turbulence (CAT) can occur. Because of the stratosphere's dryness and stable mean temperature structure, mean turbulence levels are generally very low (Nastrom and Eaton 1997; Alisse et al. 2000), and thus it is often mistakenly believed that severe CAT is never an issue for flights at these altitudes. Though much U-2 flight history remains classified, it has emerged that CAT was implicated in the loss of a U-2 over Korea and numerous other mishaps (Allen 2003), and nearly a half-century of accumulated U-2 pilot experience has revealed that, away from deep convective tropical weather, severe turbulence encounters at altitude usually occur near mountains (see, e.g., Ehernberger 1987; Stefanutti et al. 1999). The only plausible connection between underlying topography and severe in-flight CAT in the dry, generally stable middle stratosphere at ~20 km is via the direct communication of mountain-generated gravity waves (mountain waves) from the ground to the stratosphere, where they break and generate turbulence.

Thus forecasts of stratospheric mountain wave CAT are required, but current operational numerical weather prediction (NWP) models cannot provide them. Finite computational resources mean that these models cannot be run at the ultrafine-scale space-time resolutions necessary to explicitly resolve both the full spectrum of gravity waves forced by flow across complex topography and the even smaller turbulent layers that form within breaking waves (Kim et al. 2003).

* Corresponding author address: Stephen D. Eckermann, E. O. Hulburt Center for Space Research, Code 7646, Naval Research Laboratory, Washington, DC 20375; e-mail: stephen.eckermann@nrl.navy.mil

Report Documentation Page

Form Approved
OMB No. 0704-0188

1. REPORT DATE	2. REPORT TYPE	3. DATES COVERED
JUN 2004		**00-00-2004 to 00-00-2004**

4. TITLE AND SUBTITLE	5a. CONTRACT NUMBER
The NRL Mountain Wave Forecast Model (MWFM)	5b. GRANT NUMBER
	5c. PROGRAM ELEMENT NUMBER
6. AUTHOR(S)	5d. PROJECT NUMBER
	5e. TASK NUMBER
	5f. WORK UNIT NUMBER
7. PERFORMING ORGANIZATION NAME(S) AND ADDRESS(ES) **Naval Research Laboratory,Middle Atmosphere Dynamics Section,4555 Overlook Avenue, SW,Washington,DC,20375**	8. PERFORMING ORGANIZATION REPORT NUMBER
9. SPONSORING/MONITORING AGENCY NAME(S) AND ADDRESS(ES)	10. SPONSOR/MONITOR'S ACRONYM(S)
	11. SPONSOR/MONITOR'S REPORT NUMBER(S)

12. DISTRIBUTION/AVAILABILITY STATEMENT
Approved for public release; distribution unlimited

13. SUPPLEMENTARY NOTES
The original document contains color images.

14. ABSTRACT

15. SUBJECT TERMS

16. SECURITY CLASSIFICATION OF:			17. LIMITATION OF ABSTRACT	18. NUMBER OF PAGES	19a. NAME OF RESPONSIBLE PERSON
a. REPORT **unclassified**	b. ABSTRACT **unclassified**	c. THIS PAGE **unclassified**		**20**	

This limitation is well recognized in the NWP community through the implementation of subgridscale orographic gravity wave drag (GWD) parameterizations within global NWP models that specify the missing synoptic-scale drag forces produced by breaking mountain waves (Milton and Wilson 1996; Webster et al. 2003; Kim et al. 2003; Eckermann et al. 2004). A recent overview of these issues by Kim et al. (2003) shows no imminent prospect of increases in computing power that will permit global NWP model resolutions sufficient to resolve the full spectrum of breaking mountain waves.

In the lower atmosphere, mesoscale forecast models could be run operationally at ultrahigh resolution within special limited geographical domains (e.g., Clark et al. 2000; Benoit et al. 2002), such as specific airports near high mountains that are susceptible to downslope mountain wave-related wind storms and/or rotors (e.g., Denver, Juneau, Hong Kong). Yet even recent high-resolution mesoscale model forecast runs for some such limited domains have encountered resolution or numerical problems in predicting the mountain waves intercepted by aircraft in the region (Benoit et al. 2002; Doyle et al. 2002), highlighting the challenge this poses for conventional NWP systems.

Thus, for the foreseeable future we must seek novel new forecasting strategies for mountain wave CAT, particularly given the DoD need to do so both globally and up to mid-stratospheric altitudes that are not a traditional focus of NWP (e.g., Eckermann et al. 2004). One such alternative approach has been to feed conventional synoptic-scale forecast products generated by existing operational NWP systems into dedicated offline models that focus exclusively on the gravity wave problem. Allowing this secondary "postprocessor" model to focus solely on modeling gravity waves removes to some extent the computational constraints of runs embedded within an NWP system, permitting offline runs on external computing resources with massively enhanced spatial resolution and/or novel physics, dynamics or numerics, and the potential improvements in predictive skill that such enhancements can provide.

Several offline gravity-wave-related prediction algorithms have been developed along these lines, with most focused on solving some set of differential equations (e.g. Taylor-Goldstein equations) that yield gravity wave solutions constrained by large-scale forecast fields (e.g., Shutts 1997; Nance and Colman 2000; Vosper 2003). These models show predictive skill for the particular problems they are designed for, which tend to be regional and focused on the lower atmosphere. None of these at present forecast stratospheric gravity wave CAT globally.

The exception is the NRL Mountain Wave Forecast Model (MWFM), which was first developed in the early 1990's with the specific original goal of forecasting stratospheric mountain wave CAT for potentially hazardous polar stratospheric science flights with NASA's ER-2 (Bacmeister et al. 1994). The ER-2 is a longer, wider "extended range" version of a standard AF U-2, better suited to performing long stratospheric science flights for NASA with the added weight of onboard scientific instrumentation. The ER-2 was first used in the late 1980's to measure and research the newly discovered Antarctic Ozone Hole (Tuck et al. 1989). Such flights could have been hazardous if severe CAT was encountered over Antarctica, given the hostile remote environment. Accordingly a very conservative flight strategy was used (Tuck et al. 1989). Nonetheless, these ER-2 flights regularly intercepted stratospheric mountain waves emanating from the Antarctic Peninsula (Gary 1989): fortunately, none of these waves were turbulent. Later missions in the Northern Hemisphere, however, encountered some moderate-high stratospheric CAT, which the initial MWFM was able (via hindcasting) to

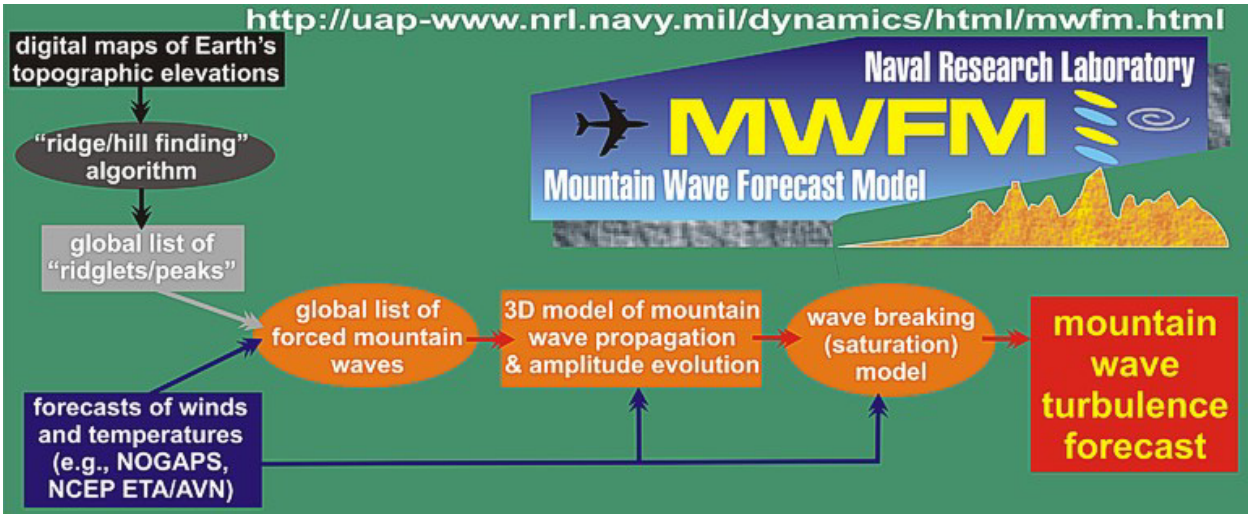

Figure 1: Schematic flowchart of the current MWFM forecasting algorithm, showing raw topography (black) reduced to a global list of diagnosed "ridgelets" (gray): see Figure 2. Forecast surface winds (blue) are blown over these ridgelets to yield a global spectrum of forced mountain waves.2D hydrostatic non-rotating (MWFM-1) or 3D nonhydrostatic rotating (MWFM-2) gravity wave/ray equations are used to model the generally oblique subsequent propagation of these mountain waves away from their parent ridges. Vertical profiles of forecast winds and temperatures are continuously fed in to these equations to model this wave evolution with altitude. A wave-breaking criterion is continually checked and, when satisfied, activates a wave breaking model and a wave-induced CAT forecast (shown in red).

associate definitiely with mountain wave breaking (Bacmeister et al. 1994).

Since then, MWFM CAT forecasts have supported flight planning for NASA airborne ER-2 science missions when and where necessary. The MWFM has now clocked up over a decade's worth of experience in forecasting stratospheric mountain wave CAT for the ER-2. The MWFM has been continuously maintained and significantly upgraded at NRL over that time: the upgrades have both significantly improved the stratospheric CAT forecasts, and yielded new forecast products such as mountain wave-induced cloud formation potential and upper tropospheric mountain wave CAT, which have both been utilized in science missions using other NASA airframes, such as the DC-8 and WB-57. More recently, the MWFM has played major new AF support roles by forecasting/hindcasting stratospheric CAT for DoD HALE aircraft before and during Operations Southern Watch, Enduring Freedom and Iraqi Freedom (Eckermann 2002). Future airborne NASA science missions will make use of HALE UAV airframes as well.

Despite this heritage, so far the MWFM has not been transitioned to any operational NWP centers. For the forecasting tasks described in this paper, the code is still run in an automated "operational" forecasting configuration that has been established and refined over many years at NRL's Space Science Division. There it automatically downloads NWP forecast fields issued by the National Centers for Environmental Prediction (NCEP) and the Navy's Fleet Numerical Meteorology and Oceanography Center (FNMOC) when they appear, then uses them to forecast mountain wave CAT as in Figure 1, issuing the final results to customers as forecast maps on the web, for example[1]. A version of the MWFM has been provided to the Air Force Weather Agency (AFWA) and is apparently being tested there using MM5 forecast winds as input, to assess its potential for their mission (Allen 2003). However, its

[1] http://uap-www.nrl.navy.mil/dynamics/html/mwfmforecasts.html

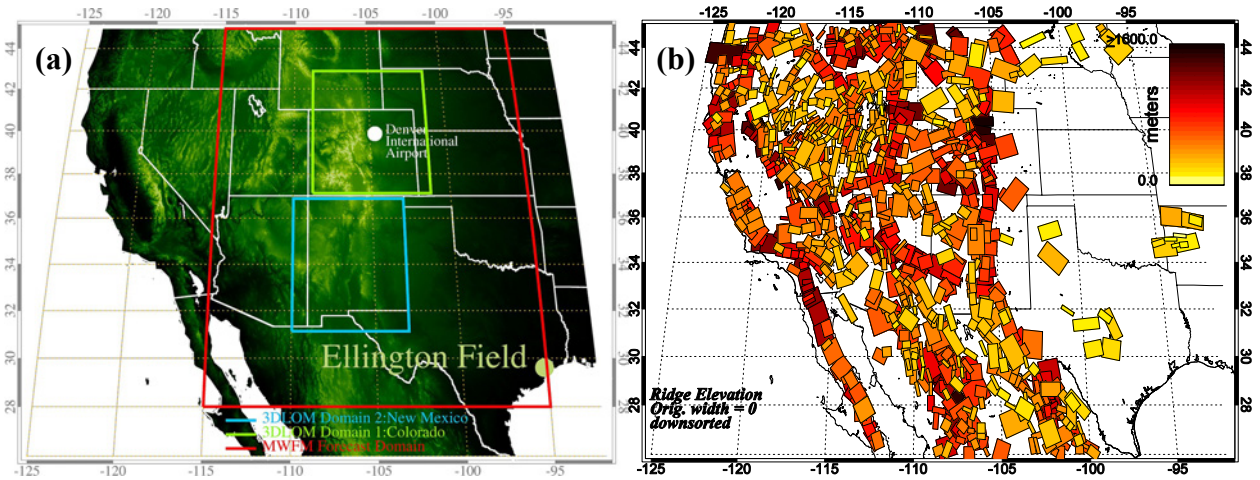

Figure 2: (a) raw topographic elevations over the western USA from the GTOPO30 digital elevation model database. Red boundary box shows domain used during operational MWFM-1 and MWFM-2 forecasting for NASA's MidCiX experiment during April-May, 2004, in which the HALE WB-57 aircraft flew science missions out of Ellington Field. (b) One of the MWFM ridgelet databases formed from ridge-based decomposition of topography for region (a). Overlapping ridges are sorted in the plot such that higher ridgelets are plotted beneath shorter ones, consistent with small peaks sitting atop larger ridges. Color coding (see top right) depicts the height of each ridgelet.

stratospheric CAT potential will remain unfulfilled until AFWA lifts the current upper boundary of its MM5 forecast model significantly higher than its current top at ~60 hPa (Allen 2003), which lies at or below typical HALE aircraft cruise altitudes. Given rapid technological advances in HALE UAVs and their emerging utility for aspects of DoD's mission and various civilian applications, we believe reliable global operational stratospheric mountain wave CAT forecasts will soon be needed as real-time decision aids for these airframes. The MWFM, appropriately transitioned, could provide this kind of capability.

Our focus in what follows is to provide a general introductory overview of the MWFM, focusing less on the mathematical details (which can be found in other publications) and more on its current status and performance as a relatively mature global forecasting tool for stratospheric mountain wave CAT. Section 2 provides a general tour through the MWFM, introducing the forecasting approach and algorithms and focusing on physical insight. Section 3 illustrates some CAT forecasting applications, focusing mainly on airborne NASA science missions for which we have the best *in situ* validation data. Section 4 concludes with an look towards the future: specifically, a developmental Version 3 MWFM, based on an entirely new Fourier-ray formulation developed at NRL, that we are now evaluating as a potential next-generation dynamical core.

2. MOUNTAIN WAVE FORECAST MODEL (MWFM)

Currently there are 2 largely separate versions of the MWFM, denoted MWFM-1 and MWFM-2. Both models are used in forecasting work, but these days we place greatest trust in the newer MWFM-2 forecasts. We still regularly consult our MWFM-1 forecasts as a consistency check, given their much longer heritage and validation in ER-2 mission forecasting. The relatively "frozen" MWFM-1 physics facilitates more effective comparisons with archived MWFM-1 forecasts from previous missions. MWFM-1 represents our standard reference product against which newer MWFM products and model enhancements are compared.

Parameterization Approach and Algorithm

The MWFM employs the quasi-analytical parameterization approach to mountain waves common within NWP models, but with significant differences in focus, implementation and complexity. The orographic GWD parameterizations in NWP models are highly simplified codes, optimized for the very specific task of computing (as rapidly as possible) average GWD profiles within a model grid box: anything extraneous to that one task is jettisoned from the code to maintain a fast efficient NWP model.

MWFM, on the other hand, runs "offline" as a remote diagnostic "postprocessor" of NWP forecast products: Figure 1 presents a simplified flowchart summarizing the basic forecasting algorithm. The offline formulation is depicted with NWP fields, shown in blue, fed in to the model's core equations (orange) to model mountain wave generation, propagation and breakdown within this forecast environment in as much physical and spatial detail as possible (e.g., no gridbox averaging). Figure 1 also shows that, in this offline configuration, these MWFM mountain wave predictions do not feed back to influence the NWP model fields. This can be justified to some extent theoretically, since gravity waves, once generated, essentially decouple from the larger-scale motion until they break (see, e.g., McIntyre and Norton 2000). Indeed, this decoupling concept is central to many core ideas in meteorology and NWP: e.g., nonlinear normal mode initialization schemes used in NWP models (Leith 1980).

The other key feature of MWFM is its topographic specification, depicted in black/gray in Figure 1, which we now explain.

Topographic Specification

The MWFM approach to topographic specification is to analyze the Earth's complex raw topography (Figures 2a and 3), identifying and characterizing those features most directly relevant to mountain wave generation by near-surface flow patterns. Many of the Earth's major topographic features approximate quasi-two-dimensional ridges (e.g., the Andes, the Shenandoahs), and flow across the short axis of these ridges efficiently forces plane (quasi-two-dimensional) mountain waves. Thus, a "ridge-finding" algorithm is applied to digital terrain elevation models (DEMs), in which the local topography is progressively fitted and decomposed into a collection of quasi-two-dimensional ridge functions, or "ridgelets." (Bacmeister et al. 1994). Figure 2b plots resulting MWFM ridgelets arising from applying one such decomposition algorithm to raw topography in the western United States, shown in Figures 2a and 3. Each ridgelet has a series of characteristics relevant to mountain wave forcing: central longitude and latitude, cross-ridge width L, peak ridge height h (color coded in Figure 2b), ridge base altitude z_b, horizontal orientation φ_{LONG} of its long ridge axis, and a normalized "ridge quality" fit parameter q, among others. This is a once-only process: various databases containing global lists diagnosed ridgelets are stored for later use in MWFM forecasting.

The ridge base altitude z_b is worth noting

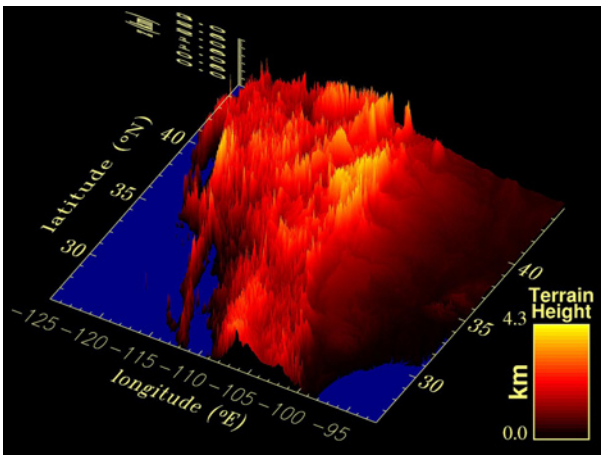

Figure 3: Raw GTOPO30 terrain elevations from Figure 2a, plotted both as a 3D surface and colored contours (see linear color bar scale, bottom-right).

here. It typically varies from ridge to ridge. For example, Figure 3 plots in surface form the raw topography shaded in Figure 2a, showing elevations above sea level of up to 4.3 km. Yet none of the ridgelets in Figure 2b have ridge heights in excess of 1.6 km, since it is the elevation of mesoscale ridge features above the broad-scale topography that is relevant for mountain wave forcing. Figure 3 shows nicely how these mesoscale features protrude upwards as peaks of ~0-1.5 km above a mean elevation of several kilometers or so: these properties are captured in the MWFM ridgelet databases through h and z_b, respectively. Moreover, since smaller narrower ridges exist as peaks atop higher wider ridges, then these former ridgelets have base heights z_b near the peak altitudes of the latter underlying ridgelets.

Our ridge databases vary with decomposition algorithm and various passbands for ridge widths L (see Bacmeister et al., 1994 for details). This can be used to add or remove ridgelets with certain properties in a given MWFM forecast. Figure 2b plots ridgelets for a combined database containing both broad and narrower width ridgelets.

Version 1 Model: MWFM-1

The major differences between MWFM-1 and MWFM-2 are in the wave forcing, propagation and breaking algorithms, depicted in orange in Figure 1.

Figure 4 depicts the way in which the MWFM-1 uses near-surface winds from NWP model output flowing across a given ridgelet (shown in red) to specify a forced mountain wave. The "surface" wind in Figure 4a is the NWP value at the ridgelet's base altitude z_b. MWFM-1 uses a two-dimensional wave generation hypothesis, which assumes that only the flow component along the cross-ridge axis, orthogonal to ridge axis (shown in red), is relevant to mountain wave generation. This cross-ridge axis is plotted in white in Figure 4a. Thus the entire problem can be two-dimensionalized by analyzing flow and ridge components along this cross-ridge axis only, as shown in Figure 4b. The ridge height determines the wave's initial vertical displacement amplitude, subject to a Froude number-dependent blocking criterion, which, when activated, reduces the effective height h of the ridgelet by raising z_b. The ridgelet width L is needed to calculate horizontal wavelengths $\lambda_{h,,}$ but is not utilized in the MWFM-1 since horizontal wavelength terms factor out of the hydrostatic wave equations: while it is technically needed to initialize the surface-level momentum flux density of the wave, that value is set using a constant "effective" L value for a given ridgelet database: see section 3c of Bacmeister et al.

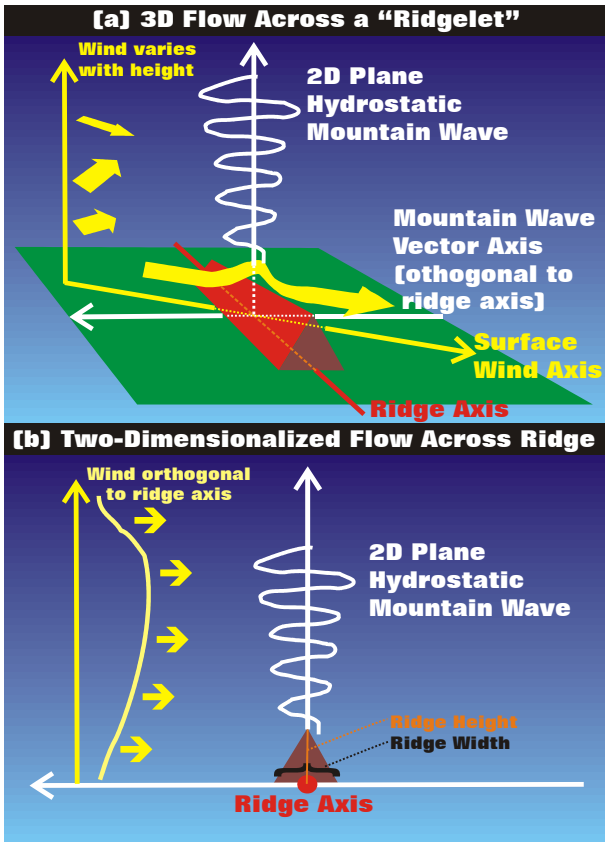

Figure 4: (a) schematic depiction of flow (yellow) across a ridgelet (red). MWFM-1 mountain wave generation is two-dimensionalized in (b) by rotating coordinates to axes orthogonal to the long ridge axis.

(1994) for details. The values of L and λ_h play much more important roles in the MWFM-2.

Given a spectrum of forced waves above all the ridgelets, MWFM-1 uses steady two-dimensional (Figure 4b) hydrostatic irrotational gravity wave equations to model the vertical propagation of gravity waves higher into the atmosphere, subject to environmental conditions specified by vertical profiles of forecast winds and temperature above the parent ridge (see Figure 1). Under these approximations, stationary mountain waves always propagate in a vertical beam directly above the ridgelet, as depicted in Figure 4. Because of this, MWFM-1 forecasts often plot their mountain wave forecasts at altitude using parent ridgelet maps, like those in Figure 2b, but with the color code now depicting the mountain wave amplitude or CAT intensity due to the 2D wave radiated directly above that ridgelet (see, e.g., Figure 8).

As waves propagate vertically, they grow in amplitude and a linear wave-overturning criterion is checked at each altitude to see if a threshold amplitude for wave breaking has been reached. If so, MWFM applies a linear saturation model (Lindzen 1981; Fritts 1984) that dissipates just enough wave momentum flux to return the wave to marginal stability, and then assumes that the dissipated wave energy and momentum flux densities are converted into inertial range three-dimensional turbulence. The saturated mountain wave continues propagating vertically in this formulation, rather than breaking down completely at its breaking level. This procedure yields a forecast mountain wave CAT intensity at that particular altitude above the ridgelet. We assume that this dissipated momentum flux density gets converted into turbulent kinetic energy (TKE), and so use the former to specify our forecast CAT intensity in J m^{-3}, a value that is taken to be proportional to (but not equal to) the final CAT TKE. One reason for not aggressively pursing a more formal turbulence derivation is that there is no straightforward correlation between CAT TKE and the degree of turbulent buffeting of any given airframe (the effects are highly airframe-specific). To date we use this same quantity and carefully cailibrate it with available U-2 PIREPS to calibrate its range for light, moderate and severe turbulent buffeting.

This procedure, iterated for all relevant ridges within a specified domain (which can be hemispheric or even global), yields geographical maps of mountain wave CAT at specifiable reference pressure altitudes, that can extend well into the stratosphere and above (Bacmeister et al. 1994).

The basic MWFM-1 discussed by Bacmeister et al. (1994) has been improved in a number of ways over time, though many of the changes are largely cosmetic or algorithmic (see section A.1.5. of Eckermann 2002). One of the more important physics upgrades was to replace a earlier pressure-based approximation of atmospheric density in the momentum flux calculation with a full hydrostatic evaluation of atmospheric density profiles from forecast NWP pressure and temperature fields, which makes the vertical amplitude evolution and wave breaking predictions significantly more accurate.

Version 2 MWFM (MWFM-2)

While MWFM-1 immediately showed some skill in forecasting stratospheric mountain wave CAT for NASA's ER-2 (Bacmeister et al. 1994; Eckermann et al. 2000a, 2000b), it was recognized from the outset that the MWFM-1 incorporated many simplifying assumptions, the more major of which were listed in section 4 of Bacmeister et al. (1994) as areas requiring further development. The MWFM-2 was developed with a view to divesting the model of several of these specific shortcomings.

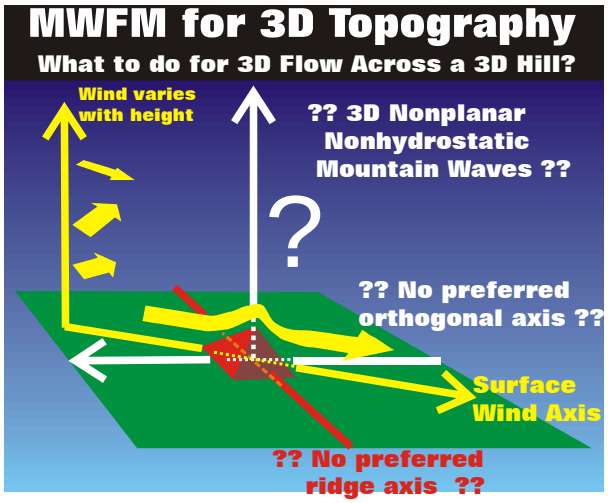

Figure 5: Problem when the 2D MWFM-1 ridge-based wave forcing algorithm is applied to a 3D hill/peak, for which no preferred ridge axis can be defined self consistently.

MWFM-2's major change is to completely replace the gravity wave dynamical core (depicted in orange in Figure 1) with a new formulation based on a general set of three-dimensional mountain wave ray-tracing equations governed by a nonhydrostatic rotating dispersion relation (Marks and Eckermann, 1995). The simplest motivation for this is illustrated by the problem three-dimensional topography presents to the 2D MWFM-1 forcing algorithm in Figure 4a. As depicted in Figure 5, flow across a purely 3D hill or mountain cannot be two-dimensionalized as in Figure 4b, because there is no preferred "ridge axis." It is well known that the situation in Figure 5 generates three-dimensional mountain waves with "ship-wave" shapes that can radiate long distances downstream (Smith 1980; Sharman and Wurtele 1983; Shutts 1998; Broutman et al. 2001; see Figure 12a). Some of the earliest work on ship mountain waves showed that spatial ray methods for gravity waves could model many of the salient aspects (Gjevik and Marthinsen 1978; Hines 1988). Further, work by Marks and Eckermann (1995) and Eckermann and Marks (1997) led to generalized global ray-tracing code for gravity waves in arbitrarily gridded numerical atmospheres that contained both nonhydrostatic and rotational wave-physics effects omitted from the MWFM-1 equations. Bacmeister et al. (1994) cited omission of nonhydrostatic effects as one of three major MWFM-1 shortcomings. Further, ray methods are computationally fast, accurate when/where valid, and yield solutions for arbitrary wind and temperature profiles (Marks and Eckermann 1995), making them attractive as a forecasting algorithm. Finally, they fit quite naturally within the MWFM forecasting flowpath structure depicted in Figure 1.

Another major motivation for moving to ray methods was the potential for ultrafine-scale geolocation of mountain wave CAT for flight planning. Such fine-scale resolution may seem counterintuitive at first, given that MWFM uses large-scale fields from NWP models, which have coarse gridbox-scale resolutions (Figure 1). However, from Figure 2b we know the actual location of ridgelets much more accurately than this, and since ray propagation paths from these ridgelets are controlled (refracted) mostly by large-scale flow patterns, this could then yield precise forecasts of wave packet locations by forecasting ray path trajectories. This sort of gain in forecast resolution via an intelligent algorithm is not unprecedented: consider, for example, parcel advection algorithms for stratospheric trace constituents, which use coarse-gridded winds to generate much finer-scale tracer filaments through the dynamical principle of downscale enstrophy transfer (e.g., Waugh and Plumb 1994; Bartello 2000).

The new MWFM-2 using 3D spatial ray-tracing was developed and validated as a research project during 1998-1999 (Eckermann and Preusse 1999) and came "online" for first forecast operations in support of NASA's SAGE III Ozone Loss and Validation (SOLVE) Experiment with the ER-2 and DC-8 aircraft flying out of Kiruna, Sweden during the Arctic winter of 1999-2000

(Newman et al. 2002). Eckermann et al. (2000a, 2000b) describe initial beneficial impacts for forecasting. Subsequent applications have shown significant increases in forecast/hindcast skill (Eckermann and Preusse 1999; Hertzog et al. 2002; Preusse et al. 2002; Pagan et al. 2004) and some detailed long-term global validation studies have been performed using emerging stratospheric mountain wave products from satellite instruments (Jiang et al. 2002, 2004). Specific examples are given in section 3.

Technical details of the current MWFM-2 ray algorithms can be found in Hertzog et al. (2002), Jiang et al. (2004), and other references therein: we provide only a brief summary here. For simplicity and ease of comparison, we use the same MWFM-1 ridgelet databases (Figure 2b). Rays are launched from these ridges at a specifiable number of I_ϕ azimuth angles distributed uniformly about the parent ridge and I_K different horizontal wavenumbers ($2\pi/\lambda_h$) based on the ridgelet width L, giving a total of $I_{TOT} = I_\phi I_K$ individual rays launched from each parent ridgelet. Typical values are $I_\phi = 6-12$ and $I_K = 2-3$. For quasi 2D ridgelets, as in Figure 4a, those rays aligned closest to the cross ridge axis are assigned the strongest initial wave amplitude and those at displaced angles receive proportionally lower initial amplitudes, whereas for purely 3D obstacles, as in Figure 5, all rays receive similar starting amplitudes. This enables the MWFM-2 to generate both plane waves from quasi-2D ridges and ship waves from circular obstacles, and all variations between these two limiting cases. The degree of ridgelet three-dimensionality is defined by the normalized ridge quality parameter q ($0 \le q \le 1$), which quantifies how closely the original topography was approximated by fitting a 2D ridge function: q~1 indicates highly 2D ridge-like topography, whereas q<<1 usually indicates a more symmetric three-dimensional (3D) obstacle. Once assigned, wave amplitudes vary along each ray's group propagation path according to conservation of the vertical flux of wave action density, subject to dissipation by dynamical and convective wave breaking thresholds [*Marks and Eckermann*, 1995]. Wave breaking is parameterized using a linear saturation hypothesis, with wave action densities scaled back accordingly. Waves are removed by both critical layers, excessive dissipation, "stalling" due to excessively slow vertical group velocities, and vertical reflection at turning points.

3. FORECASTING EXAMPLES

Here we provide a few examples of the MWFM forecasts in action: the cases we can present are restricted by space constraints for this volume. Most of the examples involve data from NASA airborne science missions, for which there are adequate in-situ data from the aircraft to permit some kind of postmission validation. A recurring problem in MWFM stratospheric CAT forecasting is a severe dearth of aircraft validation data. For example, while we have conducted numerous CAT forecasts for AF HALE aircraft, almost all of those flight paths and data remain classified and unavailable to us for any form of validation analysis.

NASA SUCCESS Flight of 2 May 1996

Figure 6a plots 3D flight paths flown on May 2, 1996 by the NASA DC-8 (red) and ER-2 (brown) during the Subsonic Aircraft Cloud and Contrail Effects Special Study (SUCCESS). Both flights took off from Salina, Kansas and headed northwest towards the Rockies, visually scouting for mountain wave clouds. Note the similar flight patterns: this occurred because the ER-2 carried nadir-viewing instruments to study the wave clouds intercepted by the DC-8, as well as any effects of DC-8 exhaust on cloud evolution. The

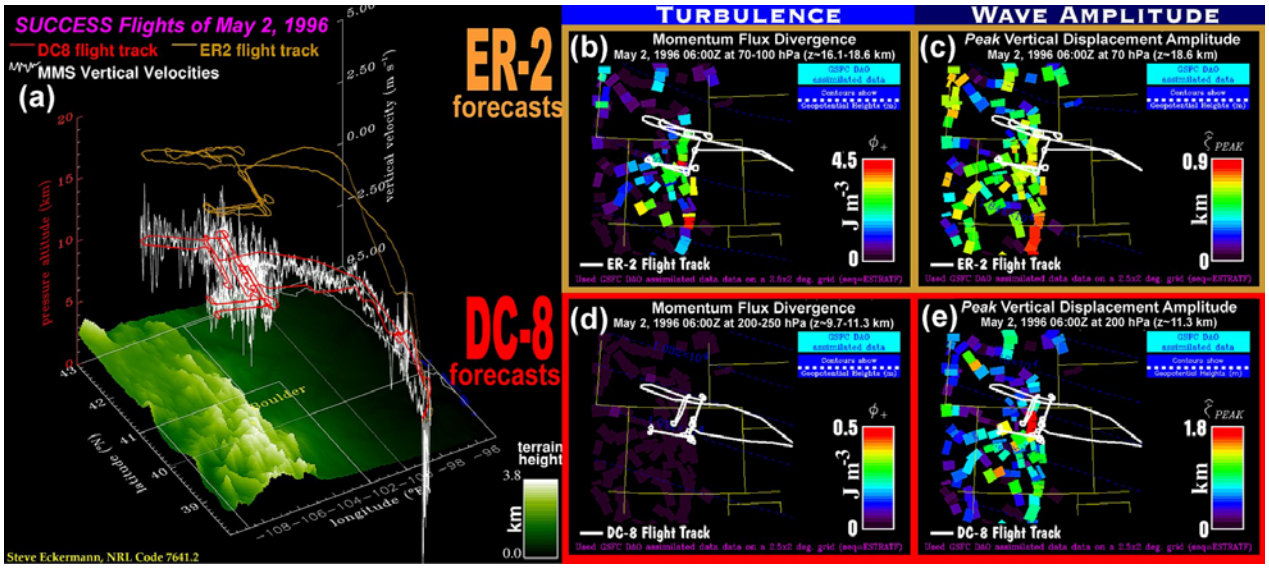

Figure 6: (a) three-dimensional plot of flight paths on May 2, 1996 by NASA's DC-8 (red curve) and ER-2 (brown curve). Underlying topographic elevations are plotted in green (see color bar). MMS vertical velocities measured on the DC-8 are plotted along the flight track in white (see axis scale). (b) MWFM-1 turbulence "forecast" (hindcast) at 70-100 hPa (heights ~16-18 km, the approximate ER-2 cruise altitude here) using GMAO assimilated data for May 2, 1996 at 06:00 UT. (c) MWFM-1 forecast of peak vertical displacement amplitudes due to mountain waves at 70 hPa. (d) MWFM-1 turbulence forecast at 200-250 hPa (heights ~10-12 km). (e) MWFM-1 forecast of peak vertical displacement amplitudes at 200 hPa. In panels (b)-(e), the relevant flight track is plotted in white, the squares correspond in each case to the ridgelet that forced this particular mountain wave, and yellow lines shown state borders.

irregularity of the flight patterns was due to the hunt for suitable wave clouds across Colorado.

The white curve superimposed on the DC-8 flight path in Figure 6a plots *in situ* 1 Hz atmospheric vertical velocities measured onboard the DC-8 by the MMS instrument. Large amplitude oscillations are evident over the Rockies, which were later analyzed by Dean-Day et al. (1998) and shown to be mountain waves. Despite the large wave activity that was intercepted, neither the DC-8 pilot nor the scientists onboard reported any unusual in-flight turbulence.

No vertical velocity measurements were acquired by the ER-2, although wave oscillations were evident in the routine navigational wind data. The ER-2 pilot, however, reported "heavy turbulence" at cruise altitudes and classified the flight afterwards as "highly turbulent."[2] Interestingly, MWFM-1 CAT forecasts were performed and made available during SUCCESS but appear not to have been utilized, apparently because tropospheric clouds and contrails were the primary focus of the mission. Thus, it is interesting to hindcast the May 2, 1996 situation using MWFM-1.

Since the NWP forecast data are no longer available, we use analyzed winds and temperatures for that day from NASA's Global Modeling and Assimilation Office (GMAO). The resulting MWFM-1 "hindcasts" are shown in the remaining panels of Figure 6. At DC-8 cruise altitudes (atmospheric pressures ~190-240 hPa for this flight, altitudes ~10-12 km), MWFM-1 predicts large mountain wave amplitudes along the flight

[2] http://cloud1.arc.nasa.gov/success/daily_summary/Flight_reports/960502.er2.html

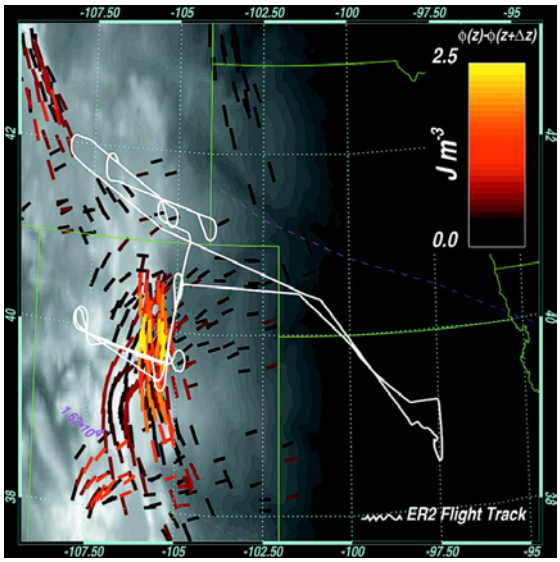

Figure 7: MWFM-2 hindcast of mountain wave CAT at 70-100 hPa on May 2, 1996 at 12:00 UT, using GMAO assimilated data of 2.5°x2° grid resolution (see dotted blue grid and purple geopotential height contours). ER-2 flight track is plotted in white, state borders in green. The line color corresponds to CAT intensity at individual ray path points, while alignment corresponds to the orientation of wave phase fronts. Gray scale shows underlying topographic elevations.

track (Figure 6e) but essentially no wave-induced turbulence (Figure 6d), consistent with the in-flight MMS data and pilot reports. Conversely, MWFM-1 hindcasts at ER-2 altitudes (pressures ~60-80 hPa on this flight) show moderate wave amplitudes (Figure 6c) but fairly intense wave-induced turbulence (Figure 6b). Experience with MWFM-1 CAT forecasts over the past decade has shown that a useful working threshold for "uncomfortable" stratospheric CAT for the ER-2 is ~1 J m^{-3} (see section 2). Many values in Figure 6b along the ER-2 flight track are well in excess of this, with a peak value of 6.4 J m^{-3} forecast 6 hours earlier (not shown). Again, these features are entirely consistent with the navigational data and pilot notes from this flight.

Figure 7 shows the CAT hindcast from the MWFM-2 model, which has interesting similarities and differences to the MWFM-1 forecast (Figure 6b). While the activity here is more limited, both in absolute magnitude and geographical coverage, here too intense turbulence occurs at the lower corner of the U-shaped ER-2 flight pattern. A significant portion of this ER-2 flight occurred in this region, with 4 separate flight segments passing through the hindcast turbulent region. Again, this hindcast is consistent with the available data from this flight.

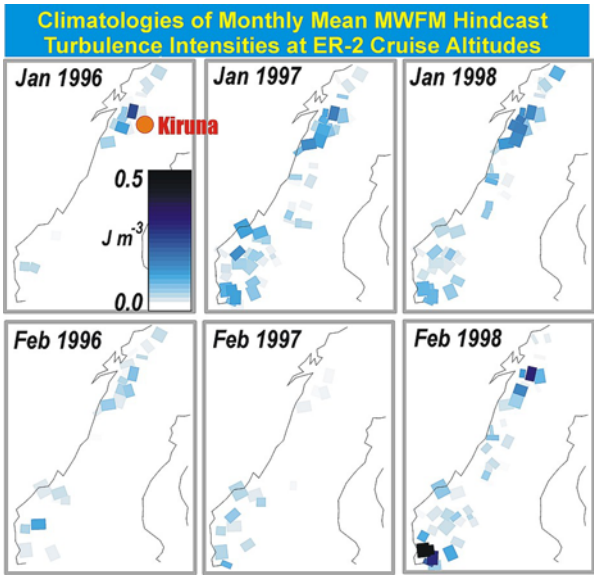

Figure 8: Monthly-average mountain wave-induced CAT at 50-70 hPa (~18-21 km) over Scandinavia for January and February of 1996-98, from daily MWFM-1 hindcasts based on 2.5°x2° STRATF assimilations at 12Z from NASA's GMAO.

CAT Climate for HALE Aircraft Deployments

The MWFM played a major role in both pre-mission and in-field flight planning for the ER-2's deployment during the SOLVE mission (Newman et al. 2002). Before the mission there was considerable concern about flying the ER-2 out of Kiruna, Sweden (68°N, 20°E), given the high Kjønas Mountains all along the spine of Scandinavia and the potential for hazardous stratospheric CAT at altitude. Indeed, an earlier deployment with the Euopean M-55 Geophysica HALE aircraft

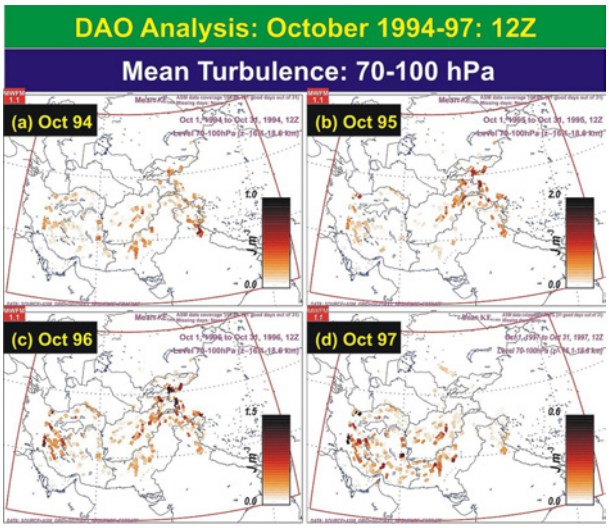

Figure 9: Monthly mean MWFM-1 CAT at 70-100 hPa for October, 1994-97 over central Asia, based on daily MWFM-1 hindcasts using daily GMAO (formerly DAO) analyses (Eckermann 2002).

recorded very intense in-flight CAT during a mountain wave intercept over Kiruna (Stefanutti et al., 1999). Thus, prior to the mission, we were tasked by NASA to hindcast the climatologically anticipated stratospheric mountain wave CAT environment in and around Scandinavia using the MWFM.

Figure 8 shows monthly mean turbulence distributions at 50-70 hPa over Scandinavia based on averaging daily MWFM-1 hindcasts. Recalling the earlier threshold for uncomfortable ER-2 CAT of ~1 J m^{-3}, these values suggest on average a light CAT environment suitable for safe ER-2 deployments. However, it also shows considerable day-to-day and interannual variability. For instance, February 1998 shows some of the largest mean CAT values near Kiruna, whereas February 1997 showed almost no CAT at all. This is consisitent with the well-known large interannual variability of the Arctic winter stratosphere (Pawson and Naujokat 1999). Beyond an overall trend for light mean turbulence, Figure 8 clearly revealed that no reliable climatological trends could be gauged for the anticipated stratospheric CAT environment, and thus twice-daily in-field MWFM CAT forecasts were ultimately required and provided.

This same kind of pre-mission climate analysis was requested by the AF Combat Climatology Center (AFCCC) very soon after September 11, 2001 when plans were rapidly set in motion to deploy both U-2 aircraft and Global Hawk HALE UAVs on reconnaissance missions over Afghanistan, a highly mountainous region. Eckermann (2002) provided a rapid summation of the anticipated stratospheric mountain wave CAT climate over this region to AFCCC and other AF clients, based on a seven year (1994-2001) average of daily MWFM-1 hindcast runs using NCEP and GMAO analyses for October-December. Figure 9 plots one of the sample CAT climate maps from Eckermann (2002), showing mean stratospheric CAT levels for October over central Asia for the years 1994-97. Again, we see fairly constant values typically in the 1-2 J m^{-3} range, which is larger and thus potentially more hazardous than over Kiruna during midwinter in Figure 9. Again, considerable interannual variability is evident, both in absolute magnitudes and in the geographical distribution of largest CAT values. As a result, "operational" MWFM-1 and MWFM-2 forecasts were provided over this region, in response to AF requests, throughout the duration of Operation Enduring Freedom.

ER-2 Ferry Flights During SOLVE

MWFM-1 and MWFM-2 forecasting for the ER-2 throughout the SOLVE mission proved extremely successful. In over 60 hours of stratospheric flying into and out of Kiruna over a wide range of high mountains throughout the polar Arctic, the ER-2 never encountered any severe turbulence, and the one brief case of moderate turbulence at altitude was over flat land in Europe, and thus

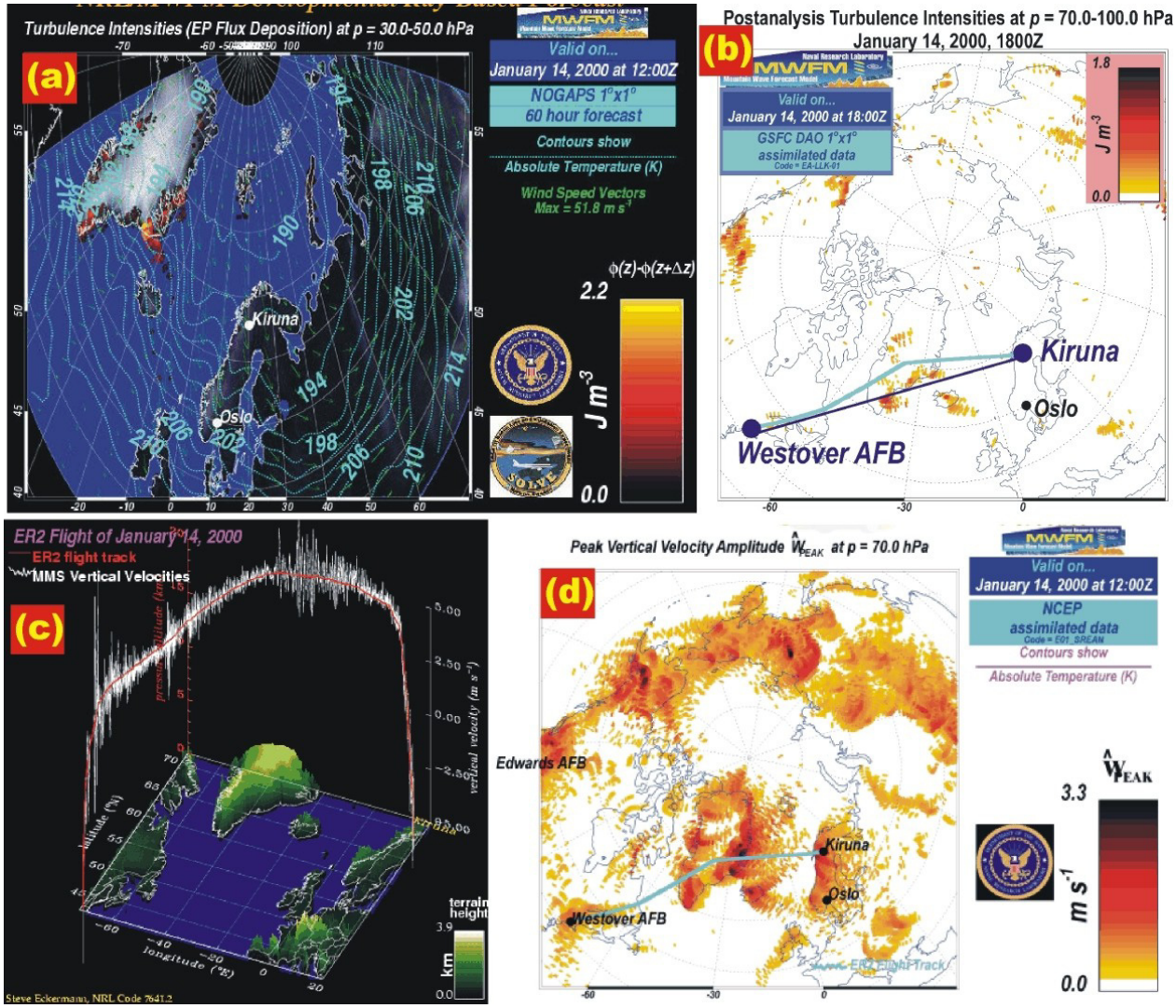

Figure 10: MWFM hindcasts for ER-2 ferry flight from Westover AFB to Kiruna on January 14, 2000: (a) +60 hour NOGAPS-initialized MWFM-2 CAT forecast, showing moderate CAT over southeastern Greenland at ER-2 cruise altitudes. Blue contours show forecast synoptic temperatures (K); (b) Hindcast MWFM-2 CAT forecast using GMAO assimilated data, showing same general structure as the archived +60 hour forecast in (a). Direct flight route (dark blue) shows likely ER-2 intercept of this turbulence. Light blue curve shows actual rerouted ER-2 flight track chosen to avoid this forecast CAT. Pilot Jan Nystrom reported no significant CAT. However, as shown in (c), large vertical velocity oscillations (~2 m s^{-1} – see right white axis) were measured by the MMS instrument over central and eastern Greenland; (d) MWFM hindcast, using NCEP reanalysis data, of peak mountain wave vertical velocity amplitudes. Peak values of ~3 m s^{-1} along the flight track over eastern Greenland compare well with MMS data in panel (c).

is unlikely to have resulted from mountain waves.

To illustrate some of the flight planning effort involved, we select the two ferry flight cases from/to Westover AF Base (AFB) in Massachusetts to/from Kiruna at the beginning/end of ER-2 deployments. An archived forecast example is shown in Figure 10a, where MWFM-2 predicted intense stratospheric CAT over south-eastern Greenland on January 14, 2000 when a "straight shot" ferry flight of the ER-2 to

Greenland was planned which would have intercepted this turbulence. Based on the MWFM-2 forecast in Figure 10a, a reroute was planned to avoid this turbulence (aqua curve in Figure 10b). The ER-2 pilot (Jan Nystrom) reported a nonturbulent flight, despite flights over higher Greenland orography and onboard measurement of stratospheric mountain wave activity over this Greenland region of ~ ±2-3 m s^{-1} (Figures 10c). To validate this MWFM-2 forecast further, Figure 10d performs an MWFM-2 hindcast of peak mountain wave vertical velocity amplitudes for this flight, with the rerouted ER-2 flight track overlaid. On comparing Figures 10c and 10d, we see excellent agreement in both the location of wave activity bursts along the ER-2 flight track and in their magnitude, with MWFM-2 hindcasting peak vertical velocity amplitudes of ~3 m s^{-1} on the eastern coast of Greenland.

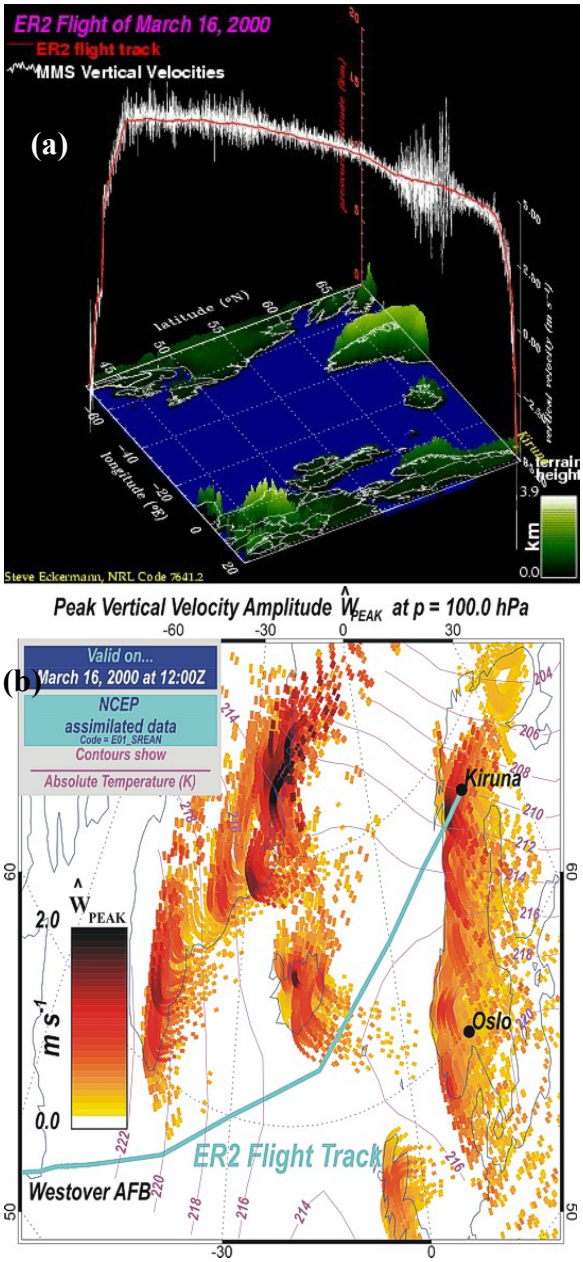

Figure 11: (a) MMS vertical velocity at altitude recorded during ER-2 ferry flight from Kiruna to Westover AFB on 16 March 2000; (b) MWFM-2 vertical velocity hindcast showing downstream ray propagation from Iceland, intercepting the ER-2 flight track over open ocean, as observed in panel (a).

Figure 11 profiles a similar hindcast for the ferry flight back to Westover AFB on 16 March 2000, which was rerouted again to avoid mountain wave CAT forecast near Iceland. Figure 11a shows enhanced vertical velocity activity measured over open ocean on the ER-2 southeast of Iceland. The MWFM-2 vertical velocity ray hindcast in Figure 11b predicts a parabolic "ship wave" pattern in stratospheric mountain wave activity, one wing of which intercepts the ER-2 at almost the exact locations along the flight track where enhancements in vertical velocity are seen in Figure 11a. Figure 11a is one of many examples of the improvements in fine scale geolocation of mountain wave activity that the new nonhydrostatic 3D ray-tracing formulation in MWFM-2 has provided for forecasting activity along HALE aircraft flight tracks.

4. THE FUTURE: MWFM-3

Ray-tracing in a Fourier-transform domain.

The considerable success we have had in implementing spatial ray methods within the MWFM-2 has motivated an ongoing parallel pure research and development effort at NRL

to extend and formalize the ray-based parameterization approach to mountain waves further (Broutman et al. 2001, 2002, 2003, 2004). This has led to a new formulation of the ray method that retains the speed and accuracy advantages of spatial ray methods but eliminates some of its shortcomings, related to caustic singularities (breakdown of the ray approximation) and use of simplified topography (Figure 2b). Our new developmental Fourier-ray model can now generate forecast wave solutions, using essentially raw DEM terrain data, that in certain situations have comparable accuracy to exact mathematical transform solutions (Broutman et al. 2003). A version of the code has now been developed for forecasting tests, which we are currently using to assess potential as a next generation dynamical core for the MWFM (MWFM-3).

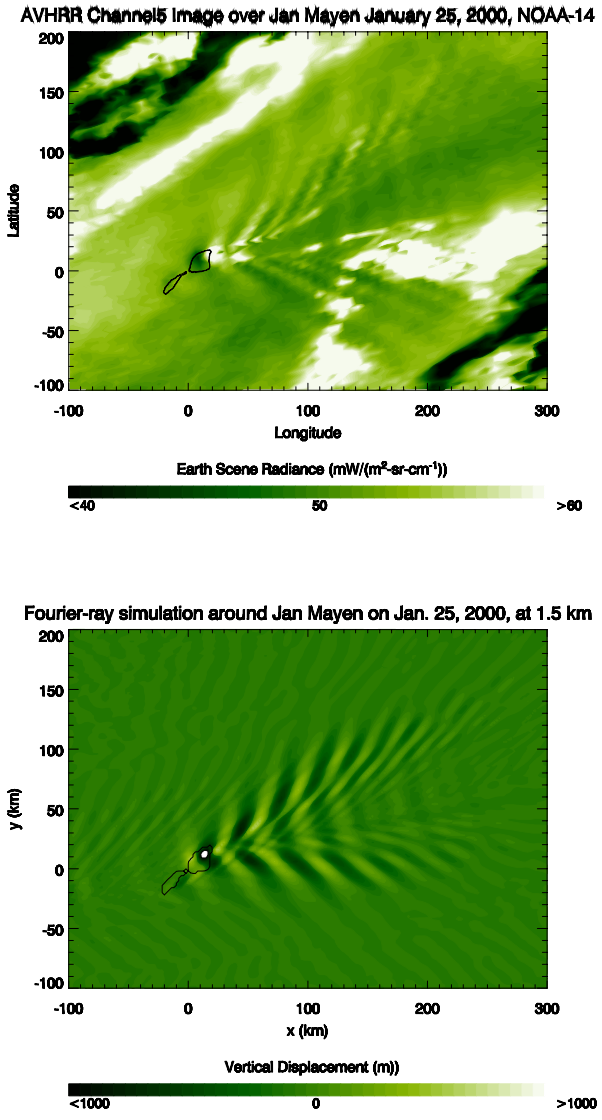

Figure 12: (a) cloud banding in the lower atmosphere downstream of Jan Mayen (71°N, 8°W observed from space in AVHRR Channel 5 infrared radiances on January 25, 2000. The "longitude" and "latitude" axes here are Cartesian distances in km, as in panel b; (b) developmental MWFM-3 hindcast of vertical displacements at z=1.5 km above sea level, using winds and temperatures from a radiosonde sounding from Jan Mayen on 25 January 2000 at 12Z. The coastline of Jan Mayen is outlined in black on both panels

Instead of tracing rays in the spatial domain, as in MWFM-2, rays here are traced in a height-varying Fourier transform domain, where the Fourier transform is taken over the horizontal wavenumbers. The ray-tracing solution is then mapped into a spatial solution (including phase) by an inverse Fourier transform. Currently we ignore horizontal gradients, so that horizontal wavenumbers are constant along each ray, as in the MWFM-2, and so the Fourier-domain ray-tracing (and caustic correction) reduces to a one-dimensional calculation as a function of the height variable. Typically we calculate the spatial solution on a grid of 1024 points in each horizontal direction and at 0.5 km height intervals from the ground to the mesosphere. This sort of calculation takes only about 1 min on a standard PC. Nonhydrostatic and non-Boussinesq effects are included. Further description of the method can be found in Broutman et al. (2002, 2003).

The calculation is most straightforward for the case of isolated topography. In Figure 12, we provide an example for mountain waves generated by flow over Jan Mayen, a small Norwegian island east of Greenland (71.0°N, 8.5°W). The topography is dominated by Mount Beerenburg (the world's northernmost volcano), which has a peak height of about 2

km above sea level and a half-width of about 5 km. Figure 12a shows a false color cloud satellite image from the Advanced Very High Resolution Radiometer (AVHRR) taken on 25 January 2000. The image shows spectacular ship-wave clouds originating from flow over Mount Beerenberg and extending many kilometers downwind. The whiter cloud decks are polar stratospheric clouds formed by cold stratospheric conditions on this day (Hervig et al. 2001; Brogniez et al. 2003). The banded clouds, however, are consistent with clouds from the lowest few kilometers of the atmosphere.

Figure 12b shows the vertical displacement field predicted by our Fourier ray-tracing model at z~1.5 km. The input wind and temperature profile for this calculation was obtained from a routine radiosonde launch from Jan Mayen on 25 January 2000 at 12Z. The similarity of the hindcast to the AVHRR imagery is strong evidence that the cloud pattern in Figure 12a is due to low-level banding produced by vertically trapped mountain waves, and that our Fourier-ray code is hindcasting this event quite accurately. The vertical trapping here is important: when trapped waves are filtered out of this forecast, the Fourier-ray prediction looks very different to the AVHRR image. The ability to fully forecast trapped wave disturbances is a potential new feature for the MWFM, since MWFM-2 simply ejects reflected waves at present.

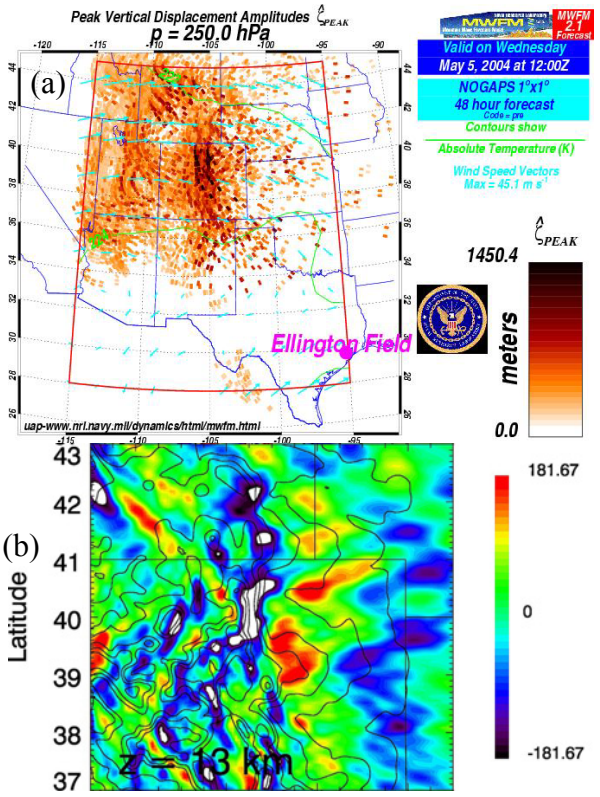

Figure 13: (a) archived operational =48 hour NOGAPS-initialized MWFM-2 forecast map of mountain wave vertical displacements for 5 may 2004. (b) Developmental Fourier-ray vertical displacement forecast at 8 km altitude over northern Colorado, valid for 5 May 2004 at 12Z based on +60 hour NOGAPS FNMOC forecasts. Color bar shows vertical displacement values in meters.

During the recent WB-57 Middle Latitude Cirrus Experiment (MidCiX) we ran this prototype MWFM-3 code in a development forecasting configuration while MWFM-1 and MWFM-2 were providing the mission-critical forecasts: an MWFM-2 example is shown in Figure 13a. We plotted Fourier-ray model forecast within two domains of interest with extended topography, centered over Colorado and New Mexico. Mean wind and buoyancy profiles were obtained from NOGAPS forecasts (Hogan and Rosmond 1991), and interpolated onto a vertical grid with 0.5 km spacing and extending from the ground to ~30 km. Forecasts were made daily, using 12, 36, 60 and 84 hour forecast fields. The topography was obtained from the GTOPO30 database (Figures 2a, 3), resampled to a 6km x-y resolution. Although we can afford plenty of extra resolution and can simulate a large mountainous region quickly, we are restricted in the present version of our model to a horizontally uniform background. We thus needed to break up the region into subdomains that are wide enough to allow sufficient horizontal propagation of the mountain waves,

yet small enough to justify our use of a horizontally uniform background.

Figure 13b shows an archived +60 hour vertical displacement Fourier-ray forecast valid for 5 May 2004 at 12Z at ~8km altitude over Colorado, for which the MWFM-2 predicted nonturbulent mountain waves over northern and central Colorado (Figure 13a) which the WB-57 subsequently flew out to and probed. Upper tropospheric mountain wave clouds were forecast and subsequently measured by instruments on the WB-57. Like the MWFM-2 forecast, this Fourier-ray forecast also yields largest mountain wave amplitudes over northern Colorado. The full computational domain here is about 4 times the width and length of the region shown. The extra space is needed because our use of an inverse Fourier transform makes the spatial solution periodic. We thus taper the mountain elevation to zero at the boundaries of the computational domain, and we also have to leave enough lateral space to prevent wrap-around errors due to the periodicity of the domain.

The amplitudes at present are much smaller than those predicted by the MWFM-2, an issue we are currently exploring. MWFM-3 includes geometrical horizontal spreading effects in its wave amplitude calculations (Broutman et al. 2001, 2002) that the MWFM-2 does not contain, which may play some role in some of the differences. However, most of the differences seem to result at present from excessive low-level blocking and mountain height reduction in our MWFM-3 surface forcing parameterization, which we are in the process of remedying Much more work is required as we further develop and validate this emerging Version 3 MWFM code, but the initial results from MidCiX are encouraging with respect to the model's stability, speed and skill when run in forecast model with inputs from operational NWP model fields.

5. ACKNOWLEDGEMENTS

This work was supported in part by the Office of Naval Research though NRL's 6.2 research program and by NASA through the ACMAP, UARP and Radiation Sciences Programs. Work in the middle-late 1990's by J. T. Bacmeister with the MWFM and support from CDR Erik Long during 1999-2000 are both gratefully acknowledged.

6. REFERENCES

Alisse, J. R., P. H. Haynes, J. Vanneste, and C. Sidi, 2000: Quantification of stratospheric mixing from turbulence microstructure measurements, *Geophys. Res. Lett*., **27**, 2621-2624.

Allen, Capt. M. S., 2003: Evaluation of the Mountain Wave Forecast Model's stratospheric turbulence simulations, M. Sc. Thesis, Department of the Air Force Air University, Air Force Institute of Technology, Wright-Patterson Air Force Base, Ohio, AFIT/GM/ENP/03-01, 81pp.

Bacmeister, J. T., 1993: Mountain-wave drag in the stratosphere and mesosphere inferred from observed winds and a simple mountain-wave parameterization scheme, *J. Atmos. Sci.*, **50**, 377-399.

Bacmeister, J. T., P. A. Newman, B. L. Gary, and K. R. Chan, 1994: An algorithm for forecasting mountain wave-related turbulence in the stratosphere, *Wea. Forecasting*, **9**, 241-253.

Bartello, P., 2000: Using low-resolution winds to deduce fine structure in tracers. *Atmos.–Ocean*., **38**, 303–320.

Benoit, R., et al., 2002: The real-time ultrafinescale forecast support during the special observing period of the MAP, *Bull. Am. Meteorol. Soc*., **83**, 85–109.

Brogniez, C., N. Huret, S. Eckermann, E. D. Rivière, M. Pirre, M. Herman, J.-Y. Balois, C. Verwaerde, N. Larsen, and B. Knudsen, 2003: Polar stratospheric cloud

microphysical properties measured by the microRADIBAL instrument on 25 January 2000 above Esrange and modeling interpretation, *J. Geophys. Res*., **108(D6)**, 8332, doi:10.1029/2001JD001017.

Broutman, D., J. W. Rottman and S. D. Eckermann, 2001: A hybrid method for analyzing wave propagation from a localized source, with application to mountain waves, *Q. J. R. Meteorol. Soc*., **127**, 129-146.

Broutman, D., J. W. Rottman, and S. D. Eckermann, 2002: Maslov's method for stationary hydrostatic mountain waves, *Q. J. Roy. Metorol. Soc*., **128**, 1159-1171.

Broutman, D., J. W. Rottman, and S. D. Eckermann, 2003: A simplified Fourier method for non-hydrostatic mountain waves, *J. Atmos. Sci*., **60**, 2686-2696.

Broutman, D., J. W. Rottman and S. D. Eckermann, 2004: Ray methods for internal waves in the atmosphere and ocean, *Ann. Rev. Fluid Mech.*, **36**, 233-253.

Businger, S., R. McLaren, R. Ogasawara, D. Simons, and R. J. Wainscoat, 2002: Starcasting, *Bull. Am. Meteorol. Soc*., **83**, 858–871.

Clark, T. L., W. D. Hall, R. M. Kerr, D. Middleton, L. Radke, F. M. Ralph, P. J. Neiman, and D. Levinson, 2000: Origins of aircraft-damaging clear-air turbulence during the 9 December 1992 Colorado downslope windstorm: Numerical simulations and comparison with observations, *J. Atmos. Sci*., **57**, 1105-1131.

Dean-Day, J., K. R. Chan, S. W. Bowen, T. P. Bui, B. L. Gary, and M. J. Mahoney, 1998: Dynamics of Rocky Mountain lee waves observed during SUCCESS, *Geophys. Res. Lett*., **25**, 1351-1354.

Doyle, J. D., H. Volkert, A. Dörnbrack, K. P. Hoinka, and T. F. Hogan, 2002: Aircraft measurements and numerical simulations of mountain waves over the central Alps: A pre-MAP test case, *Q. J. R. Meteorol. Soc.*, **128**, 2175-2184.

Eckermann, S. D., 2002: Climatology of mountain wave-induced turbulence in the stratosphere over Central Asia: October-December 1994-2001, Naval Research Laboratory Technical Memorandum, NRL/MR/7640—02-8594, May 24, 2002, 52pp.

Eckermann, S. D., and C. J. Marks, 1997: GROGRAT: A new model of the global propagation and dissipation of atmospheric gravity waves, *Adv. Space Res.*, **20(6)**, 1253-1256.

Eckermann, S. D. and P. Preusse, 1999: Global measurements of stratospheric mountain waves from space, *Science*, **286**, 1534-1537.

Eckermann, S. D., D. Broutman, and J. T. Bacmeister, 2000a: Aircraft encounters with mountain wave-induced clear air turbulence: hindcasts and operational forecasts using an improved global model, *Preprint Volume of the Ninth Conference on Aviation, Range and Aerospace Meteorology*, 456-459, American Meteorological Society, 11-15 September, Orlando, FL.

Eckermann, S. D., D. Broutman, K. A. Tan, P. Preusse and J. T. Bacmeister, 2000b: Mountain waves in the stratosphere, *NRL Review*, 73-86.

Eckermann, S. D., J. P. McCormack, L. Coy, D. Allen, T. Hogan, and Y.-J. Kim, 2004: NOGAPS-ALPHA: A prototype high-altitude global NWP model, Paper P2.6, *Preprint Vol. Symposium on the 50th. Anniversary of Operational Numerical Weather Prediction*, American Meteorological Society, 14-17 June (this issue).

Ehernberger, L. J., 1987: High-altitude turbulence for supersonic cruise vehicles, NASA Tech. Memo. 88285, 15pp.

Fritts, D. C., 1984: Gravity wave saturation in the middle atmosphere: A review of theory

and observations, *Rev. Geophys*., **22**, 275-308.

Gary, B. L., 1989: Observational results using the Microwave Temperature Profile during the Airborne Antarctic Ozone Experiment, *J. Geophys. Res*., **94**, 11,223-11,231.

Gjevik, B., and T. Marthinsen, 1978: Three-dimensional lee-wave pattern, *Q. J. R. Meteorol. Soc.*, **104**, 947–957.

Hecht, J., 2004: The airborne laser shoots for ballistic missile defense, *Laser Focus World*, **40**, 105-108.

Hertzog, A., F. Vial, A. Dörnbrack, S. D. Eckermann, B. M. Knudsen, and J.-P. Pommereau, 2002: In-situ observations of gravity waves and comparisons with numerical simulations during the SOLVE/THESEO 2000 campaign, *J. Geophys. Res.*, **107(D20)**, 8292, 10.1029/2001JD001025.

Hervig, M. E., K. L. Pagan, and P. G. Foschi, 2001: Analysis of polar stratospheric cloud measurements from AVHRR, *J. Geophys. Res.*, **106**, 10,363-10,374.

Hogan, T., and T. Rosmond, 1991: The description of the Navy Operational Global Atmospheric Prediction System's spectral forecast model, *Mon. Wea. Rev*. **119**, 1186-1815.

Jiang, J. H., D. L. Wu, and S. D. Eckermann, 2002: Upper Atmosphere Research Satellite (UARS) MLS observation of mountain waves over the Andes, *J. Geophys. Res*., **107(D20)**, 10.1029/2002JD002091.

Jiang, J. H., S. D. Eckermann, D. L. Wu and J. Ma, 2004: A search for mountain waves in MLS stratospheric limb radiance from the Northern Hemisphere: data analysis and global mountain wave modeling, *J. Geophys. Res*., **109**, D03107, doi:10.1029/2003JD003974.

Lindzen, R. S. 1981: Turbulence and stress owing to gravity wave and tidal breakdown, *J. Geophys. Res*., **86**, 9707-9714.

Kim, Y.-J., S. D. Eckermann, and H.-Y. Chun, 2003: An overview of the past, present and future of gravity-wave drag parameterization for numerical climate and weather prediction models, *Atmos. Ocean,* **41**, 65-98.

Leith, C. E., 1980: Nonlinear normal mode initialization and quasi-geostrophic theory. *J. Atmos. Sci*., **37**, 958–968.

Marks, C. J., and S. D. Eckermann, 1995: A three-dimensional nonhydrostatic ray-tracing model for gravity waves: Formulation and preliminary results for the middle atmosphere, J. Atmos. Sci., 52, 1959-1984, 1995.

McIntyre, M. E., and W. A. Norton, 2000: Potential vorticity inversion on a hemisphere, *J. Atmos. Sci*., **57**, 1214–1235.

Milton, S. F., and C. A. Wilson, 1996: The impact of parameterized subgrid-scale orographic forcing on systematic errors in a global NWP model, *Mon. Wea. Rev.,* **124**, 2023-2045.

Nance, L. B., and B. R. Colman, 2000: Evaluating the use of a nonlinear two-dimensional model in doiwnslope wind forecast, *Wea. Forecasting*, **15**, 715-729.

Nastrom, G. D., and F. D. Eaton, 1997: Turbulence eddy dissipation rates from radar observations at 5–20 km at White Sands Missile Range, New Mexico, *J. Geophys. Res*., **102**, 19,495–19,505.

Newman, P. A., et al., 2002: An overview of the SOLVE/THESEO 2000 campaign, *J. Geophys. Res.*, **107(D20)**, 8259, doi:10.1029/2001JD001303.

Pagan, K. L., A. Tabazadeh, K. Drdla, M. E. Hervig, S. D. Eckermann, E. V. Browell, M. J. Legg, and P. G. Foschi, 2004: Observational evidence against mountain-wave generation of ice nuclei as a prerequisite for the formation of three NAT PSCs observed in the Arctic in early December 1999, *J. Geophys. Res*., **109**, D04312, doi:10.1029/2003JD003846.

Pawson, S., and B. Naujokat, 1999: The cold winters of the middle 1990s in the northern lower stratosphere, *J. Geophys. Res*., **104**, 14,209-14,222.

Preusse, P., A. Dörnbrack, S. D. Eckermann, M. Riese, B. Schaeler, J. T. Bacmeister, D. Broutman, and K. U. Grossmann, 2002: Space-based measurements of stratospheric mountain waves by CRISTA, 1, Sensitivity, analysis method, and a case study, *J. Geophys. Res*., 107(D23), 8178, 10.1029/2001JD000699.

Schawe, D., C.-H. Rohardt, and G. Wichmann, 2002: Aerodynamic design assessment of Strato 2C and its potential for unmanned high altitude airborne platforms, *Aerospace Design Technol*., **6**, 43-51.

Sharman, R. D., and M. G. Wurtele, 1983: Ship waves and lee waves, *J. Atmos. Sci*., **40**, 396–427.

Shutts, G., 1997: Operational lee wave forecasting, *Meteorol. Appl*., **4**, 23-25.

Shutts, G. J., 1998: Stationary gravity wave structure in flows with directional wind shear, *Q. J. R. Meteorol. Soc*., **124**, 1421–1442.

Smith, R. B., 1980: Linear theory of stratified hydrostatic flow past an isolated mountain, *Tellus*, **32**, 348–364.

Stefanutti, L., L. Sokolov, S. Balestri, A. R. MacKenzie, and V. Khattatov, 1999: The M-55 Geophysica as a platform for the Airborne Polar Experiment, *J. Atmos. Oceanic Technol*., **16**, 1303–1312.

Tuck, A. F., R. T. Watson, E. P. Condon, J. J. Margitan, and O. B. Toon, 1989: The planning and execution of ER-2 and DC-8 aircraft flights over Antarctica, August and September 1987, *J. Geophys. Res*., **94**, 11,181-11,222.

Vosper, S., 2003: Development and testing of a high-resolution mountain-wave forecasting system, *Meteorol. Appl*., **10**, 75-86.

Waugh, D. W., and R. A. Plumb, 1994: Contour advection with surgery: a technique for investigating finescale structure in tracer transport, *J. Atmos. Sci*., **51**, 530–540.

Webster, S., A. R. Brown, D. R. Cameron, and C. P. Jones, 2003: Improvements to the representation of orography in the Met Office Unified Model, *Q. J. R. Meteorol. Soc.*, **129**, 1989-2010.